# Nonlinear Frequency-Domain Analysis of the Transformation of Cortical Inputs by a Motoneuron Pool-Muscle Complex

Renato Naville Watanabe and André Fabio Kohn

***Abstract*— Corticomotor coherence in the beta and/or gamma bands has been described in different motor tasks, but the role of descending brain oscillations on force control has been elusive. Large-scale computational models of a motoneuron pool and the muscle it innervates have been used as tools to advance the knowledge of how neural elements may influence force control. Here, we present a frequency domain analysis of a NARX model fitted to a large-scale neuromuscular model by the means of generalized frequency response functions (GFRF). The results of such procedures indicated that the computational neuromuscular model was capable of transforming an oscillatory synaptic input (e.g., at 20 Hz) into a constant mean muscle force output. The nonlinearity uncovered by the GFRFs of the NARX model was responsible for the demodulation of an oscillatory input (e.g., a beta band oscillation coming from the brain and forming the input to the motoneuron pool). This suggests a manner by which brain rhythms descending as command signals to the spinal cord and acting on a motoneuron pool can regulate a maintained muscle force. In addition to the scientific aspects of these results, they provide new interpretations that may further neural engineering applications associated with quantitative neurological diagnoses and robotic systems for artificial limbs.**

***Index Terms*— Corticomuscular coherence, computational model, beta-band oscillations, generalized frequency response functions, force control.**

## I. Introduction

DURING the execution of a given motor task, the motoneurons (MN) receive inputs from several sources. These inputs are normally associated with fluctuations of the motor output since a subset of them provides common synaptic inputs to a large number of MNs [1], [2]. Different frequency bands of the motor output fluctuations are often associated with different input sources. For example, alpha-band (6 Hz-12 Hz) frequencies are sometimes attributed to proprioceptive feedback [3], while beta-band (13 Hz-30 Hz) [4] frequencies are often associated with cortical oscillations transmitted to the MNs [5].

As there is no direct technique to measure the MN pool synaptic inputs in humans [6], this hinders the investigation of the roles of different frequency components of the synaptic inputs. Fortunately, the use of computational models can be very useful to study the relationship between the synaptic inputs and the MN pool output. In the last years, some biologically large-scale computational models have been developed [2], [7]–[9]. These models were used with success to reproduce and explain some motor behaviors [10] and clarified some aspects of the transduction of the premotoneuronal inputs into force [9], [11]–[14].

Despite the difficulties in measuring MN inputs, they have been (roughly) estimated by magnetoencephalography (MEG) [15], electroencephalography (EEG) [16], and local field potentials (LFP) [5], while the motor output is normally estimated by surface or intramuscular electromyogram (EMG) [17]. Using these signals, several studies reported corticomuscular coherence in the beta-band during isometric and low-frequency modulated contractions using different techniques [18]–[24]. This corticomuscular coherence indicates that muscular activity at this frequency band is due, at least in part, to descending inputs acting on the MN pool.

It has long been accepted that MN spiking behavior is primarily influenced by common synaptic inputs [1]. Recent experimental and modeling studies [2], [25], [26] suggested that the pool of MNs acts as a linear system and that the neural drive to the muscle units (MUs) reflects the common synaptic input to the MNs. This concept, together with the data on corticomuscular coherence in the beta-frequency band raises an important question about the role of beta oscillations in force control [4], since the muscle as a force generator acts as a low-pass filter of the MN spikes in a bandwidth from zero to about 5 Hz [25]. It should be noted that the apparent paradox of a coexistence of corticomuscular coherence in the beta-band (for example) and the suggested linearity of the MN pool was raised in [2], [25], and [26]. These authors

Manuscript received June 4, 2016; revised March 2, 2017; accepted April 30, 2017. Date of publication May 4, 2017; date of current version November 6, 2017. This work was supported in part by grants from the São Paulo Research Foundation (FAPESP) under Grant 2011/17193-0 and in part by the National Council for Scientific and Technological Development under Grant 303313/2011-0. The work of R. N. Watanabe was supported in part by a grant from FAPESP under Grant 2011/21103-7 and in part by a grant from both the Coordination for the Improvement of Higher Education Personnel and FAPESP under Grant 2015/21819-3. *(Corresponding author: Renato Naville Watanabe.)*

R. N. Watanabe is with the Biomedical Engineering Program, Federal University of ABC, São Bernardo do Campo, SP 09606-045, Brazil, and also with the Biomedical Engineering Laboratory, Escola Politécnica, University of São Paulo, São Paulo 05508-010, Brazil (e-mail: renato.watanabe@ufabc.edu.br).

A. F. Kohn is with the Biomedical Engineering Laboratory, Escola Politécnica, University of São Paulo, São Paulo, Brazil.

Digital Object Identifier 10.1109/TNSRE.2017.2701149

conjectured that there could be a way for a demodulation of oscillatory inputs (as beta or gamma waves) to the MN pool to occur [25]. Indeed, a recent large-scale neuromuscular model simulation study found empirically that oscillatory inputs (e.g., at beta or gamma bands) to a MN pool model caused an increase in the mean value of a force generated by the corresponding muscle model [27]. However, as this empirical finding could not be set in a more quantitative basis (due to complexity of the large-scale neuromuscular model), the motivation of the present study was exactly to try to provide a more quantitative description of the input-output mapping effected by a MN pool and the muscle it innervates.

The approach that was adopted here consisted of a nonlinear system identification of a large-scale computational model of a motoneuron pool and its innervated muscle [8], [10], [14]. Frequency domain features of the resulting NARX model were analyzed by means of a generalized frequency response function analysis (GFRF) [28]. The hypothesis was that a frequency domain analysis of the NARX model could be helpful to clarify if beta (or gamma) band oscillations occurring at the MN inputs could influence force control.

## II. Methods

The work presented here was based on two different elements. The first is the concept of Generalized Frequency Response Function (GFRF), used to analyze nonlinear systems in the frequency-domain. The second is a large-scale computational model of a MN pool and the innervated muscle. A NARX model of the latter was obtained by nonlinear identification methods [29] and is used in this work to obtain the GFRFs. In a second step, the large-scale computional model is used to test the predictions derived from the GFRFs.

### A. System Identification

The contents of this subsection are described in details in [29].

The type of model used in the motor unit pool identification was the polynomial representation of the nonlinear autoregressive with exogenous input (NARX) model [28]:

$$y(k) = \theta_0 + \sum_{i_1=1}^{n} \theta_{i_1} x_{i_1}(k) + \sum_{i_1=1}^{n} \sum_{i_2=i_1}^{n} \theta_{i_1 i_2} x_{i_1}(k) x_{i_2}(k) + \ldots + \sum_{i_1=1}^{n} \cdots \sum_{i_l=i_{l-1}}^{n} \theta_{i_1 i_2 \ldots i_l} x_{i_1} x_{i_2} \ldots x_{i_l} \quad (1)$$

where $\theta_{i_1 i_2 \ldots i_m}$ are the respective model coefficients and

$$x_m(k) = \begin{cases} u(k-m) & 1 \leqslant m \leqslant m_u \\ y(k-(m-m_u)) & mu+1 \leqslant m \leqslant m_u + m_y \end{cases} \quad (2)$$

with $u$ and $y$ the input and output signals, respectively.

The model identification of the motor unit pool was performed using the multiple forward regression orthogonal least squares algorithm (MFROLS) technique of system identification with the error reduction ratio (ERR) criterium to select the model terms [28]. This technique was chosen because the structure of the model was not known *a priori*. While most of the identification techniques require previous knowledge of the nonlinearity structure [30], [31], the MFROLS algorithm conducts an exhaustive search in a set of candidate terms and selects the most important terms of this set according to the ERR criterium [28]. After the selection of the model terms, the values of the coefficients $\theta_{i_1 i_2 \ldots i_m}$ were found by the least squares method.

### B. Generalized Frequency Response Function

The concept of frequency analysis is widely used in the analysis of linear systems. An extension of the concept of frequency response function to nonlinear systems, the GFRF, was defined in [32]. By using a NARX, it is possible to determine the GFRFs of the system. An alternative form to write the structure of a NARX model is in Eq. (3):

$$y(k) = \sum_{n=1}^{L} \sum_{p=0}^{n} \sum_{m_1,\ldots,m_n=1}^{L} c_{pq}(m_1, \ldots, m_n) \left[ \prod_{i=1}^{p} y(k-m_i) \right] \cdot \left[ \prod_{i=p+1}^{p+q} u(k-m_i) \right], \quad \text{with } p+q=n \quad (3)$$

where $L$ is the maximal order of nonlinearity of the combinations of signals $u$ and $y$, $m_i$ are the lags of the correspondent input or output signals and $c_{pq}$ are the model coefficients.

The recursive method used to obtain the GFRFs from a NARX model from Eq. (3) is presented in Eq. (4) and explained in detail in [28]. For each order of nonlinearity in the model (order 1 is for linear term, order 2 has terms in second powers or products of input and output, etc), there is a corresponding GFRF $H_n$ of order $n$. In the equations below $f_s$ is the sampling frequency, in Hz.

$$\begin{aligned} &\left\{ 1 - \sum_{m_1=0}^{L} c_{10}(m_1) e^{-j(\omega_1+\ldots+\omega_n)m_1/f_s} \right\} H_n(j\omega_1, \ldots, j\omega_n) \\ &= \sum_{m_1,\ldots,m_n=1}^{L} c_{0n}(m_1, \ldots, m_n) e^{-j(\omega_1 m_1+\ldots+\omega_n m_n)/f_s} \\ &\quad + \sum_{q=1}^{n-1} \sum_{p=1}^{n-q} \sum_{m_1,\ldots,m_n=1}^{L} \\ &\quad \times \left\{ c_{pq}(m_1, \ldots, m_n) e^{-j(\omega_{n-q+1} m_{p+1}+\ldots+\omega_n m_{p+q})/f_s} \cdot \right. \\ &\quad \left. \cdot H_{n-q,p}(j\omega_1, \ldots, j\omega_{n-q}, m_1, \ldots, m_p) \right\} \\ &\quad + \sum_{p=2}^{n} \sum_{m_1,\ldots,m_p=1}^{L} c_{p0}(m_1, \ldots, m_p) H_{n,p} \\ &\quad \times (j\omega_1, \ldots, j\omega_n, m_1, \ldots, m_p) \end{aligned} \quad (4)$$

where:

$$\begin{aligned} &H_{n,p}(j\omega_1, \ldots, j\omega_n, m_1, \ldots, m_p) \\ &= \sum_{i=1}^{n-p+1} H_i(j\omega_1, \ldots, j\omega_i)\, H_{n-i,p-1}(j\omega_{i+1}, \ldots, j\omega_n) \\ &\quad \cdot e^{-j(\omega_1+\ldots+\omega_i)m_p} \end{aligned} \quad (5)$$

with:

$$H_{n,1}(j\omega_1,\ldots,j\omega_n,m_1)=H_n(j\omega_1,\ldots,j\omega_n)e^{-j(\omega_1+\ldots+j\omega_n)m_1} \tag{6}$$

The algorithm that implements Eq. (4), Eq. (5) and Eq. (6) was written in MATLAB® (MathWorks®) language, used the Symbolic Math Toolbox™ (MathWorks®) and can be found in https://github.com/rnwatanabe/FROLSIdentification.

By analyzing the GFRFs of a system, it is possible to predict some system behaviors. The value of the GFRF of order $n$, $H_n(f_1, f_2, \ldots, f_n)$ is the (complex) gain of the system having inputs with frequency components at $f_1, f_2, \ldots, f_n$, which can be positive or negative. The output signal frequency corresponding to these inputs will be $f_1 + f_2 + \ldots + f_n$. The Fourier transform of the output signal $y(k)$ can be written as a function of the GFRFs and the spectrum of the input signal using the following equation [28]:

$$\begin{aligned} Y(f) &= \sum_{n=1}^{\infty} Y_n(f) \\ Y_n(f) &= \left(\frac{1/\sqrt{n}}{(2\pi)^{n-1}}\right) \\ &\quad \cdot \left(\int_{f=f_1+\ldots+f_n} H_n(f_1,\ldots,f_n)\prod_{i=1}^{n} U(f_i)\,d\sigma_{f_n}\right) \end{aligned} \tag{7}$$

where $Y_n(f)$ is the Fourier transform of the fraction of the output signal corresponding to the terms in the identified model of order $n$; $U(f)$ is the Fourier transform of the input signal; $d\sigma_{f_n}$ denotes an infinitesimal area on the hyperplane $f = f_1 + \ldots + f_n$.

### C. The Large-Scale Neuromuscular Computational Model

An existing multi-scale model of the neuromuscular system [8], [14], [33] was used in the present work to evaluate the effects of beta-band oscillations at the MNs' inputs. Here only part of the model structure was used (see Fig. 1). All the parameter values were the same used in [14]. The differential equations were solved by a fourth-order Runge-Kutta method with 0.05 ms as the integration step.

Briefly, the neuromuscular system model is composed of a motor unit pool, representing the motor nucleus of the soleus and the innervated muscle fibers. Each of the 900 MNs is modeled by the dynamics associated with voltage and neurotransmitter dependent ionic channels. Hence the output of each MN is a spike train and its inputs are time-varying synaptic conductances (which generate postsynaptic potentials). 400 descending axons connect synaptically to approximately 30% of the MNs, chosen randomly for each run. Each motor unit encompasses a MN and an associated MU [see Fig. 1(a)]. The spiking activities of the descending axons are modeled as independent Poisson point processes [see Fig. 1(b)]. The MN models are conductance-based with two compartments to represent the MN soma and the dendritic tree [see Fig. 1(c)]. The force produced by each MU is obtained by the convolution of the respective MN spike trains with the impulse response of a second-order critically damped system (which approximates a MU twitch). The signal obtained by the convolution is passed by a nonlinear saturation and multiplied by the maximal force of that muscle unit [see Fig. 1(d)]. All the individual MU signals are summed to obtain the muscle force. More details can be found in [8], [14], and [33], including model validations at different levels.

### D. Motoneuron Pool System Identification

The system identification using the MFROLS algorithm was performed using as input signal the synaptic conductance of a MN that was made to receive all the 400 descending axons, and the muscle force as the system output. Here, both the input and output signals were normalized by the mean values obtained during a simulation equivalent to a maximal voluntary contraction. The data were first low-pass filtered by an eighth-order lowpass Chebyshev zero-phase filter with a cutoff frequency of 160 Hz and then downsampled to 400 Hz. This sampling frequency was chosen based on the autocorrelation of the squared output criterium explained in [34]. The set of candidate terms was built with all possible combinations of the signals $u$ and $y$ with the maximal order of a polynomial term in Eq. (1) being seven. By using the sum of the ERR criterium [28], the values $m_u = 10$ and $m_y = 4$ were obtained.

### E. GFRFs Determination and Test

Starting from the NARX model found using the method in Subsection II-A, the GFRFs $H_n(\omega_1, \ldots, \omega_n)$ can be found from Eq. (4), Eq. (5) and Eq. (6). Regarding the question of the putative effects of beta oscillations at the input of the model, an oscillatory signal of 20 Hz was used at the MN pool inputs [27]:

$$u(t) = \begin{cases} 0.25, & 0 \leqslant t < 60s \\ 0.25 + 0.1\sin(20\pi t), & 60s \leqslant t \leqslant 120s \end{cases} \tag{8}$$

This signal was used in Eq. (7) to obtain an estimate of the output signal in the frequency-domain. An equivalent signal (interspike intervals of the descending commands with mean of 65 Hz and sinusoidal oscillation magnitude of 20 Hz) was used as a mean rate modulation of the spike train inputs to the large-scale neuromuscular computational model (see Fig. 1) to verify the predictions obtained from the use of Eq. (7).

## III. Results

The terms of the NARX model for the soleus muscle, as well as their coefficient values, are given in Table I. The time-step of this model is 0.2 ms and the input and output signals are normalized. It is interesting to notice that there is an 18 ms transport delay between input and output in the identified model. This correlates quite well with the delay caused by the propagation of action potentials along the MN axons until they reach the muscle fibers.

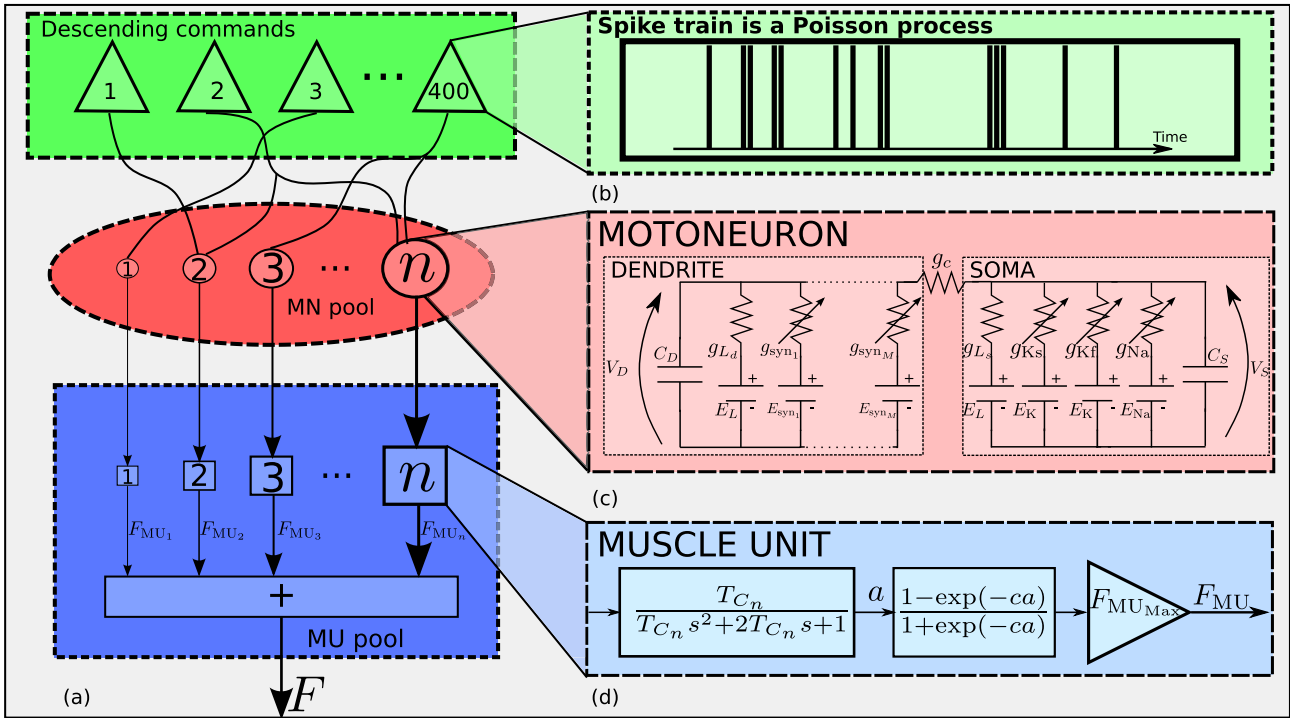


Fig. 1. Structure of the neuromuscular model used in this study. (a) schematic view of the motor unit pool. Each motor unit encompasses one motoneuron (MN) and the respective muscle unit (MU). The muscle force results from the sum of the forces of the individual muscle units; (b) train of renewal point-process representing a train of spikes of a descending axon; (c) equivalent circuit used to represent each MN model. $g_{syn_1}$ to $g_{syn_M}$:synaptic conductances for synapse 1 to $M$, respectively; $g_c$: coupling conductance; $g_{Ld}$ and $g_{Ls}$: dendritic and somatic leakage conductances, respectively; $g_{Na}$, $g_{Kf}$ and $g_{Ks}$: conductances of $Na^+$, fast $K^+$ and slow $K^+$, respectively; $E_L$: leakage Nernst potential; $E_{Na}$: and $E_K$: $Na^+$ and $K^+$ equilibrium potentials, respectively; $E_{syn_1}$ to $E_{syn_M}$: reversal potentials for synapses 1 to $M$, respectively; $C_s$ and $C_D$: somatic and dendritic capacitances, respectively; $V_S$ and $V_D$: somatic and dendritic membrane potentials, respectively. (d) block diagram of the force generation by a single MU (it encompasses a linear system and a nonlinear saturation).

TABLE I
TERMS OF THE NARX MODEL OF THE INPUT-OUTPUT BEHAVIOR OF THE MN POOL COMPUTATIONAL MODEL AND THEIR COEFFICIENTS

| Terms | Coefficients |
|---|---|
| y(k-1) | 2.16 |
| y(k-2) | -1.48 |
| y(k-3) | $4.55.10^{-1}$ |
| y(k-4) | $-1.37.10^{-1}$ |
| u(k-9) | $6.68.10^{-5}$ |
| u(k-10) | $2.41.10^{-5}$ |
| u(k-6)u(k-7)u(k-8) | $-6.53.10^{-3}$ |
| u(k-6)u(k-6)u(k-7)y(k-2) | $-4.0210^{-3}$ |
| u(k-6)u(k-6)u(k-7)u(k-7)u(k-8) | $1.14.10^{-1}$ |
| u(k-6)u(k-7)u(k-7)u(k-8)y(k-1) | 6.77 |
| u(k-6)u(k-7)u(k-7)u(k-8)y(k-3) | 8.06 |
| u(k-6)u(k-7)u(k-7)u(k-8)y(k-2) | -14.8 |
| u(k-6)u(k-6)u(k-7)u(k-7)u(k-7)y(k-1) | 43.5 |
| u(k-6)u(k-6)u(k-7)u(k-7)u(k-7)y(k-2) | -85.8 |
| u(k-6)u(k-6)u(k-7)u(k-7)u(k-7)y(k-3) | 42.1 |
| u(k-6)u(k-6)u(k-7)u(k-8)u(k-9)y(k-1) | -14.5 |
| u(k-6)u(k-6)u(k-7)u(k-8)u(k-9)y(k-3) | 14.6 |

The GFRFs $H_1(f_1)$, $H_2(f_1, f_2)$, $H_3(f_1, f_2, f_3)$, $H_4(f_1, f_2, f_3, f_4)$, $H_5(f_1, f_2, f_3, f_4, f_5)$ and $H_6(f_1, f_2, f_3, f_4, f_5, f_6)$ computed from the NARX model in Table I are given in Eq. (9), Eq. (10), Eq. (11), Eq. (11), Eq. (12), Eq. (13) and Eq. (14), respectively, as shown at the top of the next page.

These GFRFs are shown in Fig. 2, Fig. 3, Fig. 4, Fig. 5 and Fig. 6, except for $H_2(f_1, f_2)$, as it resulted a null function. The frequency axes of these graphs are colored as a function of the input signal frequency. Besides the axes, the curve ($n = 1$) and the surfaces ($n > 1$) representing the absolute values of the GFRFs are plotted with colors indicating the output signal frequency as a function of the input signal frequencies indicated on the axes and the graph titles. Points on the surface of any of the given GFRF graphs that have the same color correspond to combinations of input frequencies (positive or negative) that map onto the same output frequency. The GFRF of first order corresponds to the traditional frequency response function of a linear system and it is clear that the highest gain of $H_1$ resulted for $f_1 = 0$ Hz. The gain decreases with the increase of the input frequency, characterizing a lowpass effect. Analyzing the GFRF of third order (see Fig. 3), a similar behavior is observed. The highest gain (the darkest color) corresponds to a plane given by $f_1 + f_2 + f_3 = 0$. This means that, for this order of representation, the corresponding gain will be highest if the input signal frequencies sum up to zero. The gain decreases with an increase (or decrease) of the sum of the input frequencies from value 0.

It is interesting to note that the GFRFs make it possible to predict certain behaviors of the identified system. Particularly, one should note an increase in the mean force level ($f = 0$ Hz) in the presence of a sinusoidal signal applied at the MN pool input (Fig. 7). Fig. 7(a) shows the estimate of the output signal spectrum (absolute value) when $u(t) = 0.25$, *i.e.*, without the 20 Hz oscillation (this corresponds to a

$$H_1(f_1) = \frac{\left(1.4\cdot 10^{-15}\right)\, e^{-0.094\, f_1\, j}\, \left(\left(4.9\cdot 10^{15}\right)\, e^{0.016\, f_1\, j} + 1.8\cdot 10^{15}\right)}{1.4\cdot 10^4 + \left(1.5\cdot 10^5\right)\, e^{0.031\, f_1\, j} + \left(1.0\cdot 10^5\right)\, e^{0.063\, f_1\, j} - \left(2.2\cdot 10^5\right)\, e^{0.047\, f_1\, j} - \left(4.5\cdot 10^4\right)\, e^{0.016\, f_1\, j}} \tag{9}$$

$$H_2(f_1, f_2) = 0 \tag{10}$$

$$H_3(f_1, f_2, f_3) = -\frac{\left(6.5\cdot 10^{-3}\right)\, e^{(-0.094\, f_1\, j - 0.11\, f_2\, j - 0.13\, f_3\, j)}}{1.0 + 1.5\, e^{-0.031(f_1+f_2+f_3)j} + 0.14\, e^{-0.063(f_1+f_2+f_3)j} - 0.45\, e^{-0.047(f_1+f_2+f_3)j} - 2.2\, e^{-0.016(f_1+f_2+f_3)j}} \tag{11}$$

$$H_4(f_1, f_2, f_3, f_4) = -\frac{e^{-0.125\, f_1\, j - 0.094\, f_2\, j - 0.094\, f_3\, j - 0.11\, f_4\, j}\, \left(2.7\cdot 10^{-2}\, e^{0.016\, f_1\, j} + 9.7\cdot 10^{-3}\right)}{\left[\begin{array}{l}\left(1.0 - 2.2\, e^{-0.016(f_1+f_2+f_3+f_4)j} + 1.5\, e^{-0.031(f_1+f_2+f_3+f_4)j} + \right. \\ \quad \left. + 0.14\, e^{-0.063(f_1+f_2+f_3+f_4)j} - 0.45\, e^{-0.047(f_1+f_2+f_3+f_4)j}\right) \cdot \\ \cdot \left(1.4\cdot 10^4 + 1.5\cdot 10^5\, e^{0.031\, f_1\, j} + 1.0\cdot 10^5\, e^{0.063\, f_1\, j} - 2.2\cdot 10^5\, e^{0.047\, f_1\, j} - 4.5\cdot 10^4\, e^{0.016\, f_1\, j}\right)\end{array}\right]} \tag{12}$$

$$H_5(f_1, f_2, f_3, f_4, f_5) = \frac{\left[\begin{array}{l} 0.11\, e^{(-0.094\, f_1\, j - 0.094\, f_2\, j - 0.11\, f_3\, j - 0.11\, f_4\, j - 0.13\, f_5\, j)} + \\ \frac{\left(9.2\cdot 10^{-15}\right)\, e^{-0.11\, f_1\, j - 0.094\, f_2\, j - 0.11\, f_3\, j - 0.11\, f_4\, j - 0.13\, f_5\, j}\, \left(\left(4.9\cdot 10^{15}\right)\, e^{0.016\, f_1\, j} + 1.8\cdot 10^{15}\right)}{1.4\cdot 10^4 + \left(1.5\cdot 10^5\right)\, e^{0.031\, f_1\, j} + \left(1.0\cdot 10^5\right)\, e^{0.063\, f_1\, j} - \left(2.2\cdot 10^5\right)\, e^{0.047\, f_1\, j} - \left(4.5\cdot 10^4\right)\, e^{0.016\, f_1\, j}} + \\ + \frac{\left(1.1\cdot 10^{-14}\right)\, e^{-0.14\, f_1\, j - 0.094\, f_2\, j - 0.11\, f_3\, j - 0.11\, f_4\, j - 0.13\, f_5\, j}\, \left(\left(4.9\cdot 10^{15}\right)\, e^{0.016\, f_1\, j} + 1.8\cdot 10^{15}\right)}{1.4\cdot 10^4 + \left(1.5\cdot 10^5\right)\, e^{0.031\, f_1\, j} + \left(1.0\cdot 10^5\right)\, e^{0.063\, f_1\, j} - \left(2.2\cdot 10^5\right)\, e^{0.047\, f_1\, j} - \left(4.5\cdot 10^4\right)\, e^{0.016\, f_1\, j}} - \\ - \frac{\left(2.0\cdot 10^{-14}\right)\, e^{-0.13\, f_1\, j - 0.094\, f_2\, j - 0.11\, f_3\, j - 0.11\, f_4\, j - 0.13\, f_5\, j}\, \left(\left(4.9\cdot 10^{15}\right)\, e^{0.016\, f_1\, j} + 1.8\cdot 10^{15}\right)}{1.4\cdot 10^4 + \left(1.5\cdot 10^5\right)\, e^{0.031\, f_1\, j} + \left(1.0\cdot 10^5\right)\, e^{0.063\, f_1\, j} - \left(2.2\cdot 10^5\right)\, e^{0.047\, f_1\, j} - \left(4.5\cdot 10^4\right)\, e^{0.016\, f_1\, j}} \end{array}\right]}{\left[\begin{array}{l} 1.0 + (1.5)\, e^{-0.031(f_1+f_2+f_3+f_4+f_5)j} + \left(1.4\cdot 10^{-1}\right)\, e^{-0.063(f_1+f_2+f_3+f_4+f_5)j} - \\ - \left(4.5\cdot 10^{-1}\right) e^{-0.047(f_1+f_2+f_3+f_4+f_5)j} - (2.2)\, e^{-0.016(f_1+f_2+f_3+f_4+f_5)j} \end{array}\right]} \tag{13}$$

$$H_6(f_1, f_2, f_3, f_4, f_5, f_6) = \frac{\left[\begin{array}{l} \frac{\left(2.6\cdot 10^{-5}\right)\, e^{-0.094\, f_1\, j - 0.11\, f_2\, j - 0.13\, f_3\, j}\, e^{-0.031\, f_1\, j - 0.031\, f_2\, j - 0.031\, f_3\, j}\, e^{-0.094\, f_4\, j - 0.094\, f_5\, j - 0.11\, f_6\, j}}{1.0 + 1.5\, e^{-0.031(f_1+f_2+f_3)j} + 0.14\, e^{-0.063(f_1+f_2+f_3)j} - 0.45\, e^{-0.047(f_1+f_2+f_3)j} - 2.2\, e^{-0.016(f_1+f_2+f_3)j}} + \\ + \frac{\left(2.0\cdot 10^{-14}\right)\, e^{-0.114\, f_1 - 0.094\, f_2\, j - 0.094\, f_3\, j - 0.11\, f_4\, j - 0.13\, f_5\, j - 0.14\, f_6\, j}\, \left(\left(4.9\cdot 10^{15}\right)\, e^{0.016\, f_1\, j} + 1.8\cdot 10^{15}\right)}{1.4\cdot 10^4 + \left(1.5\cdot 10^5\right)\, e^{0.031\, f_1\, j} + \left(1.0\cdot 10^5\right)\, e^{0.063\, f_1\, j} - \left(2.2\cdot 10^5\right)\, e^{0.047\, f_1\, j} - \left(4.5\cdot 10^4\right)\, e^{0.016\, f_1\, j}} - \\ - \frac{\left(2.0\cdot 10^{-14}\right)\, e^{-0.110\, f_1\, j}\, e^{-0.094\, f_2\, j - 0.094\, f_3\, j - 0.11\, f_4\, j - 0.13\, f_5\, j - 0.14\, f_6\, j}\, \left(\left(4.9\cdot 10^{15}\right)\, e^{0.016\, f_1\, j} + 1.8\cdot 10^{15}\right)}{1.4\cdot 10^4 + \left(1.5\cdot 10^5\right)\, e^{0.031\, f_1\, j} + \left(1.0\cdot 10^5\right)\, e^{0.063\, f_1\, j} - \left(2.2\cdot 10^5\right)\, e^{0.047\, f_1\, j} - \left(4.5\cdot 10^4\right)\, e^{0.016\, f_1\, j}} + \\ + \frac{\left(5.7\cdot 10^{-14}\right)\, e^{-0.094\, f_2\, j - 0.094\, f_3\, j - 0.11\, f_4\, j - 0.11\, f_5\, j - 0.11\, f_6\, j}\, e^{-0.141\, f_1\, j}\, \left(\left(4.9\cdot 10^{15}\right)\, e^{0.016\, f_1\, j} + 1.8\cdot 10^{15}\right)}{1.4\cdot 10^4 + \left(1.5\cdot 10^5\right)\, e^{0.031\, f_1\, j} + \left(1.0\cdot 10^5\right)\, e^{0.063\, f_1\, j} - \left(2.2\cdot 10^5\right)\, e^{0.047\, f_1\, j} - \left(4.5\cdot 10^4\right)\, e^{0.016\, f_1\, j}} + \\ + \frac{\left(5.9\cdot 10^{-14}\right)\, e^{-0.094\, f_2\, j - 0.094\, f_3\, j - 0.11\, f_4\, j - 0.11\, f_5\, j - 0.11\, f_6\, j}\, e^{-0.110\, f_1\, j}\, \left(\left(4.9\cdot 10^{15}\right)\, e^{0.016\, f_1\, j} + 1.8\cdot 10^{15}\right)}{1.4\cdot 10^4 + \left(1.5\cdot 10^5\right)\, e^{0.031\, f_1\, j} + \left(1.0\cdot 10^5\right)\, e^{0.063\, f_1\, j} - \left(2.2\cdot 10^5\right)\, e^{0.047\, f_1\, j} - \left(4.5\cdot 10^4\right)\, e^{0.016\, f_1\, j}} - \\ - \frac{\left(1.2\cdot 10^{-13}\right)\, e^{-0.094\, f_2\, j - 0.094\, f_3\, j - 0.11\, f_4\, j - 0.11\, f_5\, j - 0.11\, f_6\, j}\, e^{-0.125\, f_1\, j}\, \left(\left(4.9\cdot 10^{15}\right)\, e^{0.016\, f_1\, j} + 1.8\cdot 10^{15}\right)}{1.4\cdot 10^4 + \left(1.5\cdot 10^5\right)\, e^{0.031\, f_1\, j} + \left(1.0\cdot 10^5\right)\, e^{0.063\, f_1\, j} - \left(2.2\cdot 10^5\right)\, e^{0.047\, f_1\, j} - \left(4.5\cdot 10^4\right)\, e^{0.016\, f_1\, j}} \end{array}\right]}{\left[\begin{array}{l} 1.0 - 2.2\, e^{-0.016(f_1+f_2+f_3+f_4+f_5+f_6)j} + 1.5\, e^{-0.031(f_1+f_2+f_3+f_4+f_5+f_6)j} \\ +0.14\, e^{-0.063(f_1+f_2+f_3+f_4+f_5+f_6)j} - 0.45\, e^{-0.047(f_1+f_2+f_3+f_4+f_5+f_6)j} \end{array}\right]} \tag{14}$$

mean force level around 15% of the maximum contraction). Fig. 7(b) shows the output signal spectrum considering an input $u(t) = 0.1\sin(2\pi 20t) + 0.25$. The output component at 0 Hz is higher (approximately 270) than that (approximately 175) in Fig. 7(a)), obtained when the input was only a constant signal. Also, we can observe in Fig. 7(b) that the estimate of the output spectrum shows a minute component at 20 Hz.

These predictions obtained by using Eq. (7) were replicated in the results obtained from simulations of the large-scale neuromuscular model, as shown in Fig. 7(c). In this simulation, the mean firing rate of the descending commands (independent stochastic point processes) was constant up to 60 s and the generated muscle force resulted around 350 N. After 60 s, the mean rate of the descending commands began to oscillate at 20 Hz. With the 20 Hz input oscillation, the resulting muscle force (a steady value except for the noisiness) increased to approximately 450 N.

## IV. Discussion

The nonlinear frequency domain analysis of generalized frequency response functions was applied to a NARX description of a large-scale neuromuscular model. Its results pointed to a hitherto unrecognized nonlinearity that provides a mechanism for the demodulation of oscillatory inputs typically sent down to the spinal cord by brain areas such as the primary motor cortex [21]. The results showed that the modeled motor unit pool increased the constant level of the generated muscle force when a beta-band oscillation was applied to the MN pool inputs [27]. This result suggests a putative role for the ubiquitous oscillatory activity (e.g., at the beta-band) arriving

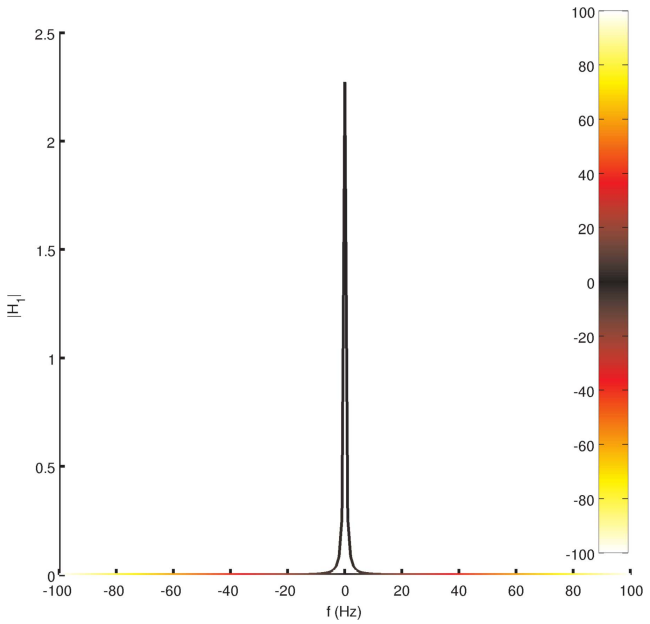


Fig. 2. Generalized frequency response functions of first order. The color of the curve represents the frequency of the output signal for the correspondent input frequency.

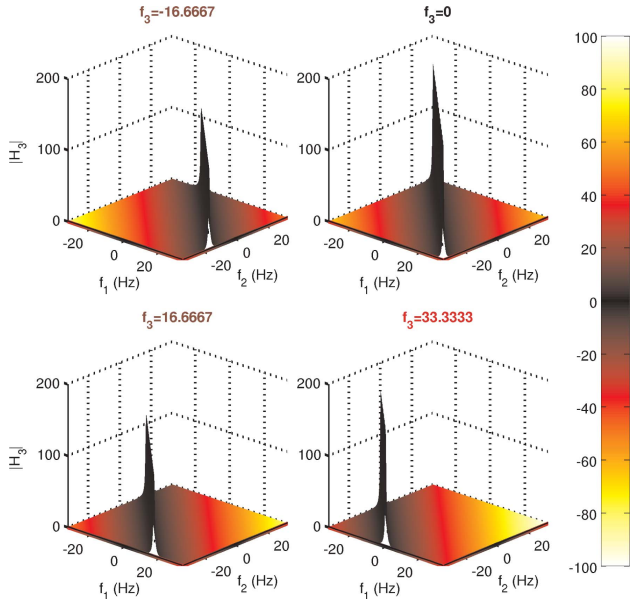


Fig. 3. Generalized frequency response functions of third order. The color of the surface represents the frequency of the output signal for the correspondent input frequencies.

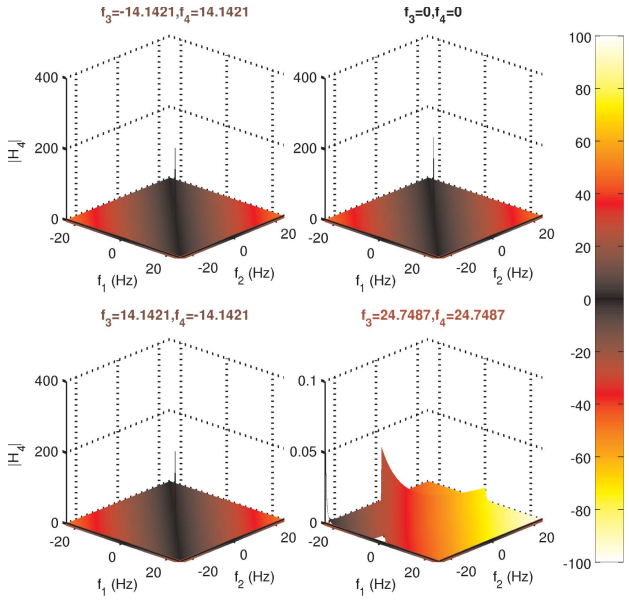


Fig. 4. Generalized frequency response functions of fourth order. The color of the surface represents the frequency of the output signal for the correspondent input frequencies.

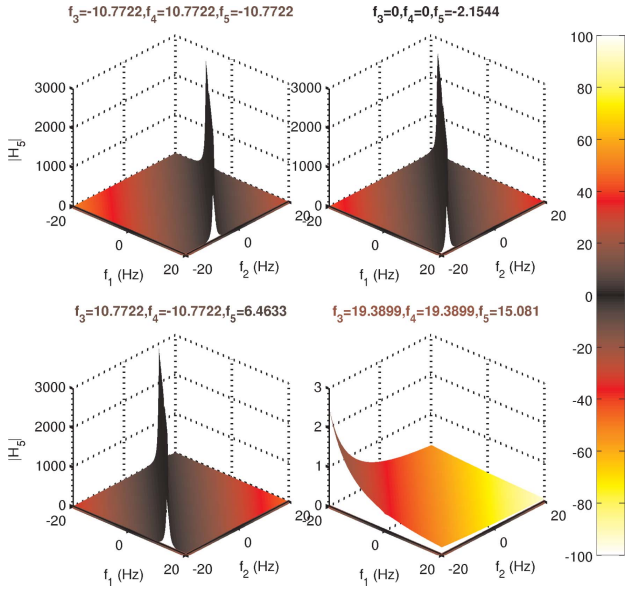


Fig. 5. Generalized frequency response functions of fifth order. The color of the surface represents the frequency of the output signal for the correspondent input frequencies.

at the spinal cord through brain descending pathways [21]: it contributes to regulate steady state force levels. While such a conclusion has been posited by some experimentally based papers [18], [35], this is perhaps the first time that this subject is studied from a bottom-up approach, by synthesizing an approximate large-scale model, obtaining a nonlinear input-output description of it and then studying the frequency domain properties of the latter.

It can be noticed that the parameter values of some of the nonlinear terms of the identified model (see Table I) have large absolute values, suggesting that a nonlinear dynamic behavior of the MN pool system may be observable for certain types of inputs. While for linear systems there is no energy transfer between frequencies, in nonlinear systems new frequency components can be generated at the output signal. It is interesting to note that a very simple manner of demodulating a high frequency oscillatory input would be to square the input signal. Therefore, we had expected to obtain second order nonlinearities. However, Table I indicates that the identified nonlinear model has no second order nonlinearities but there is a fourth order and some sixth order nonlinearities involving

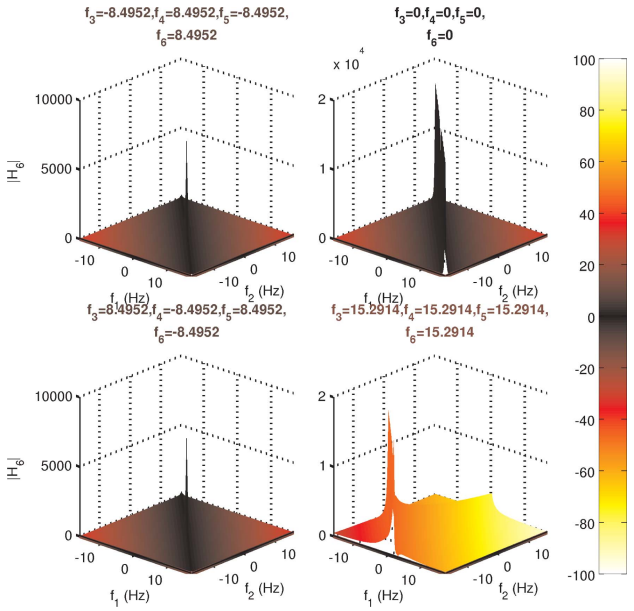


Fig. 6. Generalized frequency response functions of sixth order. The color of the surface represents the frequency of the output signal for the correspondent input frequencies.

products of input and output samples. These must contribute to generate the constant levels of muscle force. However, since their interpretation seems quite involved due to the products of delayed samples of the input and output, the GFRFs provide a more powerful quantitative tool.

As the main purpose of this work was to analyze the influence of beta-band frequency oscillations on isometric muscle contractions, a frequency domain analysis was performed using the identified system in Table I. In Fig. 3, it can be seen that the highest gain of $H_3(f_1, f_2, f_3)$ is on the plane $f_1 + f_2 + f_3 = 0$ (black color in the surfaces of Fig. 3). The same phenomenon appears for every order $n$ in Fig. 4, Fig. 5 and Fig. 6: the highest gain is on the hyperplane $f_1 + \ldots + f_n = 0$ (also in black color in the surfaces of the respective figures). This means that if the input signal has frequency components that sum up to 0 Hz (considering positive and negative frequencies), the energy contained in these frequency components will be transferred to 0 Hz and, consequently, the DC level of the output signal will increase. This phenomenon can be seen in Fig. 7 with an increase of the 0 Hz component when a 20 Hz oscillation is present at the system input, either estimated by Eq. (7) from the GFRFs (Fig. 7(a,b)) or obtained from simulation of the large-scale neuromuscular computational model (Fig. 7(c)). This effect will occur for any oscillatory frequency at the MN pool inputs. However, frequencies below approximately 5-6 Hz will also be directly transfered to the output, due to the linear part of the overall system dynamics ($H_1(f_1)$). This linear transfer does not occur for high frequency inputs, as beta or gamma band frequencies, due to the filtering by the muscle contractile and viscoelastic properties. Therefore, the special neuromuscular effect caused by the higher frequency descending commands, typically associated with motor areas of the brain, is an increase in the DC level of the force.

The prediction of such a demodulation mechanism was

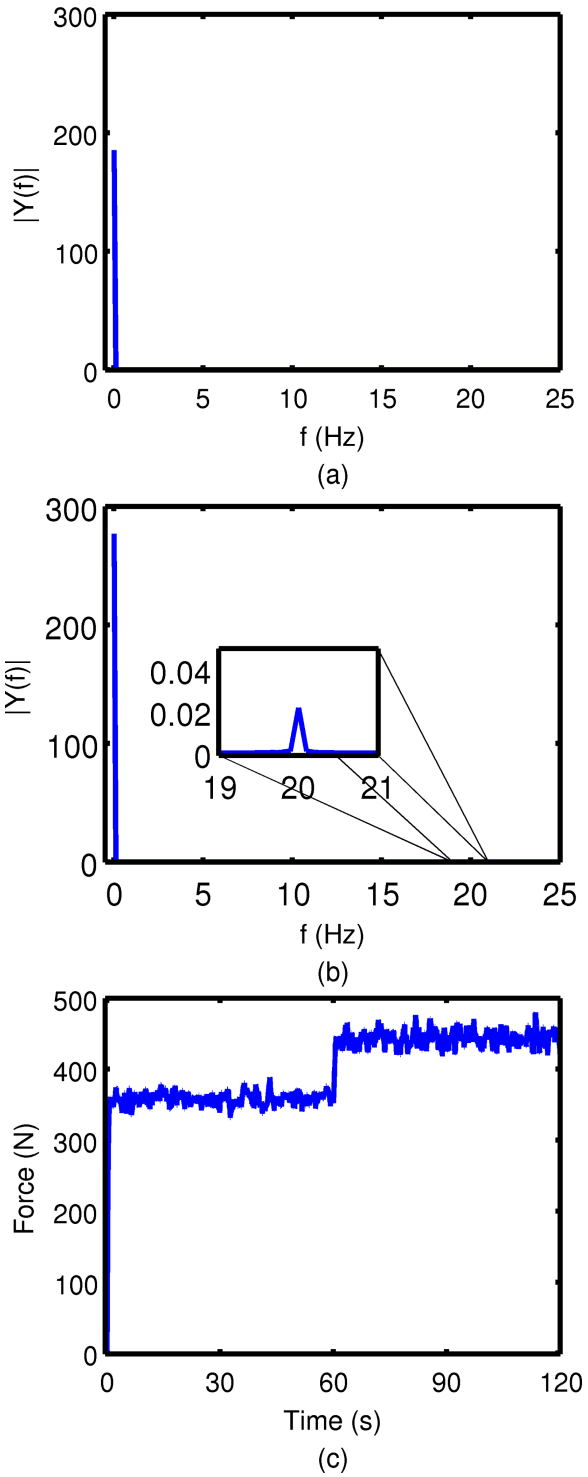


Fig. 7. Estimate of the output signal spectrum when (a) the input signal is a constant; (b) when the input signal has a 20 Hz oscillation, both for the NARX identified model. (c) Force signal obtained from the neuromuscular computational model (shown in Fig. 1).

reached when the GFRFs of the NARX equivalent model of the neuromuscular system were analyzed and interpreted. Such a transformation from an oscillatory input to a steady force level is relevant for neuroscience, since cortical oscillations in beta and gamma bands (13 Hz to 30 Hz and 35 Hz to 70 Hz, respectively) have been observed in monkeys [21], [35]–[39] and humans [4], [40]–[43] as well as in axons of the pyramidal tract of monkeys [21], in different motor tasks.

Based on previous experimental and modeling results from the literature and results from the present paper, it is possible to propose that the nervous system uses mean firing rate modulations of MN pool inputs to control time-varying forces in a linear input-output mapping, as put forward in previous research by different labs [25], [44], [45]. Additionally, the nervous system could control the basal muscle contraction level by activating/deactivating beta or gamma band oscillatory commands to the spinal cord. This would permit the control of a set-point along time, around which feedback and descending commands could develop. One of the advantages of such oscillatory commands is energy economy, but another could be a way of integrating systems of brain oscillators [4], [46] with spinal cord control of muscle behavior and sensory inflow.

These two putative modes of the MN pool behavior (linear and nonlinear) should be better investigated experimentally to pinpoint their relative importance in a behaving animal. This could also contribute to the understanding of different nervous system pathologies that affect the link between the brain and the spinal cord, as well as contribute with conceptual tools that may help design optimized brain computer interfaces.

The present NARX model analysis provided a formal demonstration of the possibility of demodulation of high frequency oscillatory inputs by a MN pool and the innervated muscle. However, the physiological mechanism cannot be grasped without computer simulations of the full neuromuscular model. Actually, a mechanism has been proposed recently [27] on the basis of computer simulations of a large-scale neuromuscular model: the mapping of a high frequency input, say 20 Hz, to steady muscle force would be due to the recruitment and derecruitment (occurring at 20 Hz) of higher threshold MNs according to the size principle [47]. Those MNs would tend to synchronize at 20 Hz and the muscle would filter out the fundamental and its harmonics, but leave the component at 0 Hz, i.e., a steady muscle force level.

A previous theoretical analysis of the response of a MN pool to oscillatory inputs [25] showed the existence of nonlinearities in the input-output mapping that generated output frequencies not existent in the input. These were weighted sums of the input frequencies and the natural frequency of the neuron model (i.e., with zero input). However, this analytical model did not predict the nonlinear behavior pointed out by the GFRFs of the present research due to the hypotheses adopted: (1) all the model neurons were already discharging, i.e., they were all recruited (so the phenomenon of recruitment and derecruitment was not represented), (2) each neuron was represented by a perfect integrator. Perfect integrator models do not phase-lock [48], [49], while most biological neurons synchronize with higher frequency inputs. Despite the poor physiological interpretability of the NARX model, it was able to encapsulate the nonlinear behavior associated with recruitment and derecruitment effects, and hence the ability of demodulation of high frequency inputs.

Pathologies in the central and peripheral nervous systems cause changes in the motor unit spike discharge patterns, which can be detected by using multichannel EMG decomposition methods based on high-density EMG [50]. The methods and results presented here, together with the sophisticated EMG signal processing methods that have been introduced recently [50], are, therefore, potentially useful to quantify the nonlinearities occurring in a given neuromuscular system. These may be used to infer what changes in the common input are taking place in different pathologies.

The coupling between descending oscillations from the cortex and the muscles has been studied by indirect means in different motor tasks by measuring the coherence between the EEG and EMG [18], [22], [35], [40]–[43], [51]–[59]. Furthermore, corticomuscular coherence have been used to assess pathologies affecting either the brain or its descending commands. The present results, together with the computer simulations shown in [27], provide an expanded view of the possibilities of interpretation of the coherence function for diagnostic purposes.

Recently, some researchers have adopted large-scale computational models as that presented in the Methods section to control robotic systems to behave similarly to neuromechanic systems [60]–[63]. The method presented here could be used to easily implement in hardware a NARX model of the complex computational neuromechanical models used to control such robotic systems.

In addition, despite the advances in the understanding of the transduction of premotoneuronal inputs into muscle force, there are many open issues. For instance, the function of Renshaw cells is still a matter of debate. Other points not completely understood are how active dendrites [64] might affect the neuromechanical transduction or how sensory inputs can influence the behavior of the MN pool. These are issues that should be revisited with new quantitative tools such as the ones applied here.

## V. Conclusion

In summary, the use of the GFRFs (together with the system identification of a NARX model) seems to be a very promising approach to the study of how forces and movements are coded by the nervous system, either in health or under a neurologic disease. Thus the techniques and results presented here provide new means for advancing research on the functioning of the nervous system as well as providing tools that may contribute to neurological diagnosis.

From the results obtained in this research, a MN pool may have a nonlinear processing mode that provides a means for the mapping of high frequency (beta or gamma-band) cortical oscillations onto steady force level. As this prediction was based on the analyses of a large-scale MN pool computational model, new experimental approaches should follow in an effort to provide additional evidence for the predicted behavior.

## References

[1] C. J. De Luca, R. S. LeFever, M. P. McCue, and A. P. Xenakis, "Control scheme governing concurrently active human motor units during voluntary contractions," *J. Physiol.*, vol. 329, no. 1, pp. 129–142, 1982.

[2] F. Negro and D. Farina, "Decorrelation of cortical inputs and motoneuron output," *J. Neurophysiol.*, vol. 106, no. 5, pp. 2688–2697, Nov. 2011.

[3] S. Erimaki and C. N. Christakos, "Coherent motor unit rhythms in the 6–10 Hz range during time-varying voluntary muscle contractions: Neural mechanism and relation to rhythmical motor control," *J. Neurophysiol.*, vol. 99, no. 2, pp. 473–483, Feb. 2008.

[4] A. K. Engel and P. Fries, "Beta-band oscillations—Signalling the status quo?" *Current Opinion Neurobiol.*, vol. 20, no. 2, pp. 156–165, Apr. 2010.

[5] S. N. Baker, J. M. Kilner, E. M. Pinches, and R. N. Lemon, "The role of synchrony and oscillations in the motor output," *Experim. Brain Res.*, vol. 128, no. 1, pp. 109–117, 1999.

[6] C. J. Heckman and R. M. Enoka, "Motor unit," *Comprehensive Physiol.*, vol. 2, pp. 2629–2682, Oct. 2012.

[7] A. H. A. Stienen, A. C. Schouten, J. Schuurmans, and F. C. T. van der Helm, "Analysis of reflex modulation with a biologically realistic neural network," *J. Comput. Neurosci.*, vol. 23, no. 3, pp. 333–348, 2007.

[8] R. R. L. Cisi and A. F. Kohn, "Simulation system of spinal cord motor nuclei and associated nerves and muscles, in a Web-based architecture," *J. Comput. Neurosci.*, vol. 25, no. 3, pp. 520–542, 2008.

[9] E. R. Williams and S. N. Baker, "Circuits generating corticomuscular coherence investigated using a biophysically based computational model. I. Descending systems," *J. Neurophysiol.*, vol. 101, no. 1, pp. 31–41, 2009.

[10] L. A. Elias, R. N. Watanabe, and A. F. Kohn, "Spinal mechanisms may provide a combination of intermittent and continuous control of human posture: Predictions from a biologically based neuromusculoskeletal model," *PLoS Comput. Biol.*, vol. 10, no. 11, p. e1003944, Nov. 2014.

[11] F. Negro and D. Farina, "Linear transmission of cortical oscillations to the neural drive to muscles is mediated by common projections to populations of motoneurons in humans," *J. Physiol.*, vol. 589, no. 3, pp. 629–637, Feb. 2011.

[12] F. Negro and D. Farina, "Factors influencing the estimates of correlation between motor unit activities in humans," *PLoS ONE*, vol. 7, no. 9, p. e44894, Sep. 2012.

[13] D. Farina, F. Negro, and N. Jiang, "Identification of common synaptic inputs to motor neurons from the rectified electromyogram," *J. Physiol.*, vol. 591, no. 10, pp. 2403–2418, Mar. 2013. [Online]. Available: http://www.ncbi.nlm.nih.gov/pubmed/23507877

[14] R. N. Watanabe, F. H. Magalhães, L. A. Elias, V. M. Chaud, E. M. Mello, and A. F. Kohn, "Influences of premotoneuronal command statistics on the scaling of motor output variability during isometric plantar flexion," *J. Neurophysiol.*, vol. 110, no. 11, pp. 2592–2606, Sep. 2013.

[15] M. Hämäläinen, R. Hari, R. J. Ilmoniemi, J. Knuutila, and O. V. Lounasmaa, "Magnetoencephalography—Theory, instrumentation, and applications to noninvasive studies of the working human brain," *Rev. Modern Phys.*, vol. 65, no. 2, pp. 413–497, 1993.

[16] E. Niedermeyer and F. L. da Silva, *Niedermeyer's Electroencephalography: Basic Principles, Clinical Applications, and Related Fields*, 4th ed. Baltimore, MD, USA: Williams & Wilkins, 1998.

[17] R. A. Mezzarane, L. A. Elias, F. H. Magalhães, V. M. Chaud, and A. F. Kohn, "Experimental and simulated EMG responses in the study of the human spinal cord," in *Electrodiagnosis in New Frontiers of Clinical Research*, H. Turker, Ed. Rijeka, Croatia: InTech, 2013, pp. 57–87.

[18] S. Salenius, K. Portin, M. Kajola, R. Salmelin, and R. Hari, "Cortical control of human motoneuron firing during isometric contraction," *J. Neurophysiol.*, vol. 77, no. 6, pp. 3401–3405, 1997.

[19] G. Pfurtscheller and F. H. L. da Silva, "Event-related EEG/MEG synchronization and desynchronization: Basic principles," *Clin. Neurophysiol.*, vol. 110, no. 11, pp. 1842–1857, Nov. 1999.

[20] M. R. Baker and S. N. Baker, "The effect of diazepam on motor cortical oscillations and corticomuscular coherence studied in man," *J. Physiol.*, vol. 546, no. 3, pp. 931–942, Dec. 2002.

[21] S. N. Baker, E. M. Pinches, and R. N. Lemon, "Synchronization in monkey motor cortex during a precision grip task. II. Effect of oscillatory activity on corticospinal output," *J. Neurophysiol.*, vol. 89, no. 4, pp. 1941–1953, 2003.

[22] J. R. Naranjo *et al.*, "Corticospinal interaction during isometric compensation for modulated forces with different frequencies," *BMC Neurosci.*, vol. 11, no. 1, p. 157, Jan. 2010.

[23] X. Wu, W. Li, S. Shen, X. Zheng, Y. Zhang, and W. Hou, "Corticomuscular coherence modulation with the pattern of finger force coordination," *IEEE Trans. Neural Syst. Rehabil. Eng.*, vol. 21, no. 5, pp. 812–819, Sep. 2013.

[24] C. van de Steeg, A. Daffertshofer, D. F. Stegeman, and T. W. Boonstra, "High-density surface electromyography improves the identification of oscillatory synaptic inputs to motoneurons," *J. Appl. Physiol.*, vol. 116, no. 10, pp. 1263–1271, May 2014.

[25] D. Farina, F. Negro, and J. L. Dideriksen, "The effective neural drive to muscles is the common synaptic input to motor neurons," *J. Physiol.*, vol. 592, no. 16, pp. 3427–3441, May 2014.

[26] D. Farina and F. Negro, "Common synaptic input to motor neurons, motor unit synchronization, and force control," *Exerc. Sport Sci. Rev.*, vol. 43, no. 1, pp. 23–33, 2015.

[27] R. N. Watanabe and A. F. Kohn, "Fast oscillatory commands from the motor cortex can be decoded by the spinal cord for force control," *J. Neurosci.*, vol. 35, no. 40, pp. 13687–13697, 2015.

[28] S. A. Billings, *Nonlinear System Identification*. Chichester, U.K.: Wiley, 2013.

[29] R. N. Watanabe and A. F. Kohn, "System identification of a motor unit pool using a realistic neuromusculoskeletal model," in *Proc. 5th IEEE RAS EMBS Int. Conf. Biomed. Robot. Biomechatronics*, São Paulo, Brazil, Aug. 2014, pp. 610–615.

[30] J. S. Bendat, *Nonlinear System Techniques and Applications*. New York, NY, USA: Wiley, 1998.

[31] D. T. Westwick and R. E. Kearney, *Identification of Nonlinear Physiological Systems*. Hoboken, NJ, USA: Wiley, 2003.

[32] D. A. George, "Continuous nonlinear systems," Dept. Elect. Eng., Massachusetts Inst. Technol., Cambridge, MA, USA, Tech. Rep. 355, 1959.

[33] L. A. Elias, V. M. Chaud, and A. F. Kohn, "Models of passive and active dendrite motoneuron pools and their differences in muscle force control," *J. Comput. Neurosci.*, vol. 33, no. 3, pp. 515–531, 2012.

[34] S. A. Billings and L. A. Aguirre, "Effects of the sampling time on the dynamics and identification of nonlinear models," *Int. J. Bifurcation Chaos*, vol. 5, no. 6, pp. 1541–1556, 1995.

[35] S. N. Baker, E. Olivier, and R. N. Lemon, "Coherent oscillations in monkey motor cortex and hand muscle EMG show task-dependent modulation," *J. Physiol.*, vol. 501, no. 1, pp. 225–241, May 1997.

[36] V. N. Murthy and E. E. Fetz, "Coherent 25- to 35-Hz oscillations in the sensorimotor cortex of awake behaving monkeys," *Proc. Nat. Acad. Sci. USA*, vol. 89, no. 12, pp. 5670–5674, 1992.

[37] V. N. Murthy and E. E. Fetz, "Synchronization of neurons during local field potential oscillations in sensorimotor cortex of awake monkeys," *J. Neurophysiol.*, vol. 76, no. 6, pp. 3968–3982, 1996.

[38] J. N. Sanes and J. P. Donoghue, "Oscillations in local field potentials of the primate motor cortex during voluntary movement," *Proc. Nat. Acad. Sci. USA*, vol. 90, pp. 4470–4474, May 1993.

[39] S. N. Baker, R. Spinks, A. Jackson, and R. N. Lemon, "Synchronization in monkey motor cortex during a precision grip task. I. Task-dependent modulation in single-unit synchrony," *J. Neurophysiol.*, vol. 85, no. 2, pp. 869–885, 2001.

[40] B. A. Conway *et al.*, "Synchronization between motor cortex and spinal motoneuronal pool during the performance of a maintained motor task in man," *J. Physiol.*, vol. 489, no. 3, pp. 917–924, 1995.

[41] J.-M. Schoffelen, R. Oostenveld, and P. Fries, "Neuronal coherence as a mechanism of effective corticospinal interaction," *Science*, vol. 308, no. 5718, pp. 111–113, 2005.

[42] R. Kristeva, L. Patino, and W. Omlor, "Beta-range cortical motor spectral power and corticomuscular coherence as a mechanism for effective corticospinal interaction during steady-state motor output," *NeuroImage*, vol. 36, no. 3, pp. 785–792, 2007.

[43] J. T. Gwin and D. P. Ferris, "Beta- and gamma-range human lower limb corticomuscular coherence," *Frontiers Human Neurosci.*, vol. 6, p. 258, Sep. 2012.

[44] D. F. Stegeman, W. J. M. van de Ven, G. A. van Elswijk, R. Oostenveld, and B. U. Kleine, "The $\alpha$-motoneuron pool as transmitter of rhythmicities in cortical motor drive," *Clin. Neurophysiol.*, vol. 121, no. 10, pp. 1633–1642, Oct. 2010.

[45] M. M. Lowery and Z. Erim, "A simulation study to examine the effect of common motoneuron inputs on correlated patterns of motor unit discharge," *J. Comput. Neurosci.*, vol. 19, no. 2, pp. 107–124, 2005.

[46] G. Buzsáki and A. Draguhn, "Neuronal oscillations in cortical networks," *Science*, vol. 304, no. 5679, pp. 1926–1929, 2004.

[47] E. Henneman, "Relation between size of neurons and their susceptibility to discharge," *Science*, vol. 126, no. 3287, pp. 1345–1347, 1957.

[48] B. W. Knight, "Dynamics of encoding in a population of neurons," *J. General Physiol.*, vol. 59, no. 6, pp. 734–766, Jun. 1972.

[49] R. B. Stein, A. S. French, and A. V. Holden, "The frequency response, coherence, and information capacity of two neuronal models," *Biophys. J.*, vol. 12, no. 3, pp. 295–322, 1972.

[50] D. Farina and A. Holobar, "Characterization of human motor units from surface EMG decomposition," *Proc. IEEE*, vol. 104, no. 2, pp. 353–373, Feb. 2016.

[51] D. M. Halliday, B. A. Conway, S. F. Farmer, and J. R. Rosenberg, "Using electroencephalography to study functional coupling between cortical activity and electromyograms during voluntary contractions in humans," *Neurosci. Lett.*, vol. 241, no. 1, pp. 5–8, 1998.
[52] T. Mima, N. Simpkins, T. Oluwatimilehin, and M. Hallett, "Force level modulates human cortical oscillatory activities," *Neurosci. Lett.*, vol. 275, no. 2, pp. 77–80, 1999.
[53] J. M. Kilner, S. N. Baker, S. Salenius, R. Hari, and R. N. Lemon, "Human cortical muscle coherence is directly related to specific motor parameters," *J. Neurosci.*, vol. 20, no. 23, pp. 8838–8845, 2000.
[54] T. Gilbertson, E. Lalo, L. Doyle, V. Di Lazzaro, B. Cioni, and P. Brown, "Existing motor state is favored at the expense of new movement during 13–35 Hz oscillatory synchrony in the human corticospinal system," *J. Neurosci.*, vol. 25, no. 34, pp. 7771–7779, 2005.
[55] A. Andrykiewicz, L. Patino, J. R. Naranjo, M. Witte, M.-C. Hepp-Reymond, and R. Kristeva, "Corticomuscular synchronization with small and large dynamic force output," *BMC Neurosci.*, vol. 8, p. 101, Nov. 2007.
[56] V. Chakarov, J. R. Naranjo, J. Schulte-Mönting, W. Omlor, F. Huethe, and R. Kristeva, "Beta-range EEG-EMG coherence with isometric compensation for increasing modulated low-level forces," *J. Neurophysiol.*, vol. 102, no. 2, pp. 1115–1120, 2009.
[57] Q. Yang, V. Siemionow, W. Yao, V. Sahgal, and G. H. Yue, "Single-trial EEG-EMG coherence analysis reveals muscle fatigue-related progressive alterations in corticomuscular coupling," *IEEE Trans. Neural Syst. Rehabil. Eng.*, vol. 18, no. 2, pp. 97–106, Apr. 2010.
[58] J. Ushiyama *et al.*, "Contraction level-related modulation of corticomuscular coherence differs between the tibialis anterior and soleus muscles in humans," *J. Appl. Physiol.*, vol. 112, no. 8, pp. 1258–1267, 2012.
[59] I. Mendez-Balbuena, F. Huethe, J. Schulte-Mönting, R. Leonhart, E. Manjarrez, and R. Kristeva, "Corticomuscular coherence reflects interindividual differences in the state of the corticomuscular network during low-level static and dynamic forces," *Cerebral Cortex*, vol. 22, no. 3, pp. 628–638, 2012.
[60] D. Farina and F. Negro, "Accessing the neural drive to muscle and translation to neurorehabilitation technologies," *IEEE Rev. Biomed. Eng.*, vol. 5, no. 1, pp. 3–14, Jan. 2012.
[61] C. M. Niu, K. Jalaleddini, W. J. Sohn, J. Rocamora, T. D. Sanger, and F. J. Valero-Cuevas, "Neuromorphic meets neuromechanics, part I: The methodology and implementation," *J. Neural Eng.*, vol. 14, p. 025001, Feb. 2017.
[62] K. Jalaleddini *et al.*, "Neuromorphic meets neuromechanics, part II: The role of fusimotor drive," *J. Neural Eng.*, vol. 101, no. 2, pp. 158–162, 2017.
[63] D. Farina *et al.*, "Man/machine interface based on the discharge timings of spinal motor neurons after targeted muscle reinnervation," *Nature Biomed. Eng.*, vol. 1, Feb. 2017, Art. no. 0025.
[64] L. A. Elias and A. F. Kohn, "Individual and collective properties of computationally efficient motoneuron models of types S and F with active dendrites," *Neurocomputing*, vol. 99, pp. 521–533, Jan. 2013.

**Renato Naville Watanabe** received the B.S. degree in electrical engineering and the M.S. and Ph.D. degrees in biomedical engineering from the University of São Paulo in 2009, 2012, and 2016, respectively. He has been a Professor with the Federal University of ABC since 2017. His research focuses on neural engineering, motor control, biomechanics of human movement and human neurophysiology by using mathematical and computational tools, such as signal processing, stochastic processes, nonlinear system identification, and control theory.

**André Fabio Kohn** received the B.S. and M.S. degrees in electrical engineering from Escola Politécnica, University of São Paulo (USP), Brazil, and the Ph.D. degree in engineering from the University of California at Los Angeles in 1980. He is a Full Professor of Electrical and Biomedical Engineering with Escola Politécnica, USP. He directs the Biomedical Engineering Laboratory with USP, where he advises students who have backgrounds either in engineering or in neuroscience. His research interests are concentrated on the neural bases of sensorimotor function in humans, involving both experimental and computer model simulation approaches.